2nd URSI AT-RASC, Gran Canaria, 28 May – 1 June 2018

Source-receiver Ionospheric-scintillation Global Model of the upper Atmosphere (SIGMA): Sensitivity Analysis

James P. Conroy(1), Kshitija Deshpande(2), Wayne Scales(1) and Amir Zaghloul*(1)
(1) Virginia Tech, Blacksburg, VA, USA
(2) Embry-Riddle, Daytona Beach, FL, USA

Abstract

We have performed a sensitivity analysis using the Source-receiver Ionospheric-scintillation Global Model of the upper Atmosphere (SIGMA) multiple phase screen based forward propagation model to explore the relationship between the number of phase screens and the convergence of amplitude and phase scintillation estimates. It was found that for highly elongated vertical irregularities that phase scintillation solutions converge when using as few as 2 or 3 phase screens while as many as 10 to 15 screens are needed for amplitude scintillation estimates to converge. It was also shown that following convergence that the addition of more screens leads to an apparent divergence of solutions which suggests a limitation to the propagation solution utilized in the current version of SIGMA. These results provide invaluable insight into the need to carefully analyze a phase screen model setup in order achieve the accuracy required for a particular application given a set of input parameters.

1 Introduction

The ionosphere is a region of the atmosphere extending from 90 to 1000 km composed of weakly ionized plasma [1]. As radio waves propagate through the ionosphere they are subjected to a variety of effects which can severely degrade global navigation satellite system (GNSS) performance. Variations in the background ionization can produce effects that are well known such as signal phase shifts and time delays [2, 3, 4]. Small-scale variations in the electron density can produce random amplitude and phase variations or scintillations [4, 5] which are often observed in GNSS signals [6, 7, 5, 8]. The study of ionospheric scintillations involves analyzing electromagnetic (EM) wave propagation in a random media [9]. In order to better understand the nature of the structures which generate scintillation we will use the Source-receiver Ionospheric-scintillation Global Model of the upper Atmosphere (SIGMA) phase screen propagation model. In this paper we use a new version of the previously developed SIGMA model [9] to complete a series of simulations using media properties thought to be representative of the polar regions and to perform a sensitivity analysis to better understand the relationship between input parameters and scintillation observables. The goal of the sensitivity study is to build upon the insight gained by [9] while exercising parameters outside the scope of that work.

SIGMA is a multiple phase screen based forward propagation model which employs a three-dimensional (3D) spectrum to generate magnetic field-aligned irregularities. SIGMA combines a multiple phase screen (MPS) simulation with the split-step method to solve the forward propagation equation (FPE) to produce realizations of the ionospheric transfer function as a function of time, space, frequency and propagation geometry for a set of irregularity parameters [9, 10, 11, 12]. While SIGMA is applicable at any latitude, it is particularly well-suited for modeling arbitrary propagation geometries in the polar regions where there is extensive vertical elongation of the irregularities along the magnetic field and a wide range of irregularity morphologies [6] that require the use of a full 3D EM wave propagation model and a highly flexible 3D power spectrum [10, 13, 14].

The basic geometry used by SIGMA to propagate a signal from a moving source to the ground through multiple phase screens is illustrated in Figure 1. The process of calculating the ionospheric transfer function is completed by propagating a spherical wave $U_0(x_0, y_0)$ from the source to the top of the irregularities, with thickness L_{th} and width L_s, which are to replaced by a series of phase changing screens. The irregularities are created by applying the 3D power spectral density P_s to Equation 1, where F^{-1} is the inverse Fourier Transform, θ_k are random numbers uniformly distributed between 0 and 1, and $\Re$ is the real part of the resulting complex numbers.

$$N_e(x,y,z) = \Re\left(F^{-1}\sqrt{P_S}\exp\left(j2\pi\theta_k\right)\right) \qquad (1)$$

While SIGMA contains several spectrum options the 3D Shkarofsky spectrum given by Equation 2 is used in this work in order to represent the irregularities with maximum flexibility [5]. σ_N^2 is the RMS of the electron density, r_0 is the inner scale or smallest irregularities in the spectrum, $l_0 = 2\pi/k_0$ is the outer scale or largest irregularities, and p is the 3D spectral index.

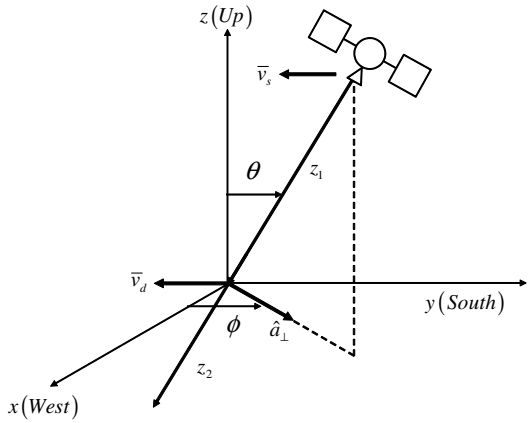

Figure 1. SIGMA coordinates centered on the ionospheric peirce point (IPP) with a satellite traveling at velocity v_s which transmits a signal that propagates through irregularities moving with a drift velocity v_d which are to be modeled as a set of phase changing screens.

$$\Phi_\xi(\mathbf{k}) = \frac{\sigma_N^2 (k_0 r_0)^{(p-3)/2} r_0^3}{(2\pi)^{3/2} K_{(p-3)/2}(k_0 r_0)} \times (r_0\sqrt{k^2+k_0^2})^{-p/2} \times K_{(p/2)}(r_0\sqrt{k^2+k_0^2}) \quad (2)$$

Axis scaling factors ax, ay, az are applied using Equation 3 to explicitly control the contribution of spatial frequencies in the 3D spectrum.

$$k^2 = \alpha_x^2 k_x^2 + \alpha_y^2 k_y^2 + \alpha_z^2 k_z^2 \quad (3)$$

Once an electron density volume is created a phase screen is calculated using Equation 4, where λ is the wavelength of the propagating signal, r_e is the classic electron radius, L_{th} is the thickness of the irregularities to be integrated, and θ is the angle of incidence [15].

$$\phi(x,y) = -\lambda r_e \sec\theta \int_{-L_{th}/2}^{L_{th}/2} N_e(x,y,z)\, dz \quad (4)$$

The calculated phase screen is applied to find the ionospheric transfer function on either the ground or the top of the next layer of irregularities using Equation 5, where f is the spatial frequency of the propagating signal in the XY plane, F is the Fourier transform, and $d_{ab} = |z_a - z_b|$ is the segment of the slant propagation path [16].

$$D(x,y) = F^{-1}\left\{ e^{j\pi\left(f_x^2+f_y^2\right)\lambda d_{21}\frac{d_{01}}{d_{02}}} F\left[e^{-j\phi(x,y)}\right](f_x,f_y)\right\} \quad (5)$$

Finally the ionspheric transfer function $D(x,y)$ is used to express the field on the ground (or at the top of the next irregularity layer) as a function of U_0 using Equation 6 [16].

$$U_2(x\frac{d_{01}}{d_{02}}, y\frac{d_{01}}{d_{02}}, z_2) = U_0(x\frac{d_{01}}{d_{02}}, y\frac{d_{01}}{d_{02}}, z_2) D(x,y) \quad (6)$$

2 Sensitivity Study

A sensitivity study was completed to investigate the relationship between the number of layers (n_{layer}), layer thickness (L_{th}), irregularity elongation, electron density fluctuations (ΔN) and the amplitude and phase scintillation indices S_4 and σ_ϕ at 1.5754 GHz. The simulations were completed with axis scaling factor α_z values of 10 and 30 in order to compare the effect of highly elongated and shorter irregularity lengths while α_x and α_y were set to unity. ΔN values ranging from 1^{11} to 10^{11} el/m^3 were used as a representative range of values as observed in polar incoherent scatter radar (ISR) data [17]. The plasma drift velocity was set to 0 m/s for experimentation purposes, the signal was normally incident on top of the irregularities from a stationary transmit satellite, and the irregularity thickness ranged from 10 to 20 km. The remaining values were set using the baseline SIGMA parameters established in [13]. The altitude of the irregularities (h_{iono}) was 120 km, and system width (L_s) was 20 km. The inner scale (r_0) was 10 m, the outer scale (l_0) was 2 km, and the 3D spectral index (spi) was 3. An example of vertically elongated electron density irregularities generated using a subset of the analyzed input parameters is included in Figure 2.

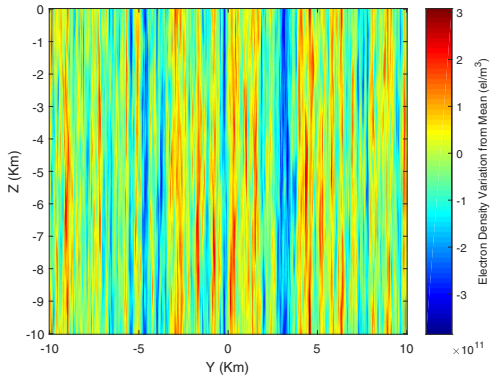

Figure 2. Vertically elongated electron density irregularities.

The results for the amplitude scintillation index (S_4) versus the number of layers for a subset of the simulated variations are included in Figure 3. These results show that for a single phase screen, a relatively high value for S_4 is initially estimated for all of the variations. As additional phase screens are added S_4 quickly reduces and effectively convergences to a constant value. For the variations where ΔN is $1^{11} el/m^3$, the resulting curves are similar expect for

a bias introduced when L_{th} is increased to 20 km. For the cases where ΔN is $10^{11} el/m^3$, the results are again similar with a bias introduced by increasing L_{th}, but converging to a constant value requires more screens for both instances.

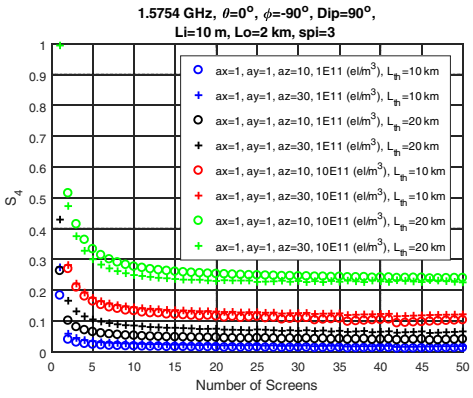

Figure 3. Results for amplitude scintillation versus the number of screens.

The results for the phase scintillation index (σ_ϕ) versus the number of layers for a subset of the simulated variations are included in Figure 4. These results show that very few phase screens are needed for σ_ϕ to converge to an effectively constant value. These results can be explained by considering that the correlation lengths in the z direction are greater than 1 km when a_z is 10 and greater than 3.5 km when a_z is 30. For the variations where ΔN is $1^{11} el/m^3$, the results are similar expect for a bias introduced by increasing L_{th} to 20 km. For the cases where ΔN is $10^{11} el/m^3$, the results are again similar but a bias is no longer introduced when L_{th} is increased. These results suggest that for these highly elongated irregularities when ΔN is large enough a saturation point is reached.

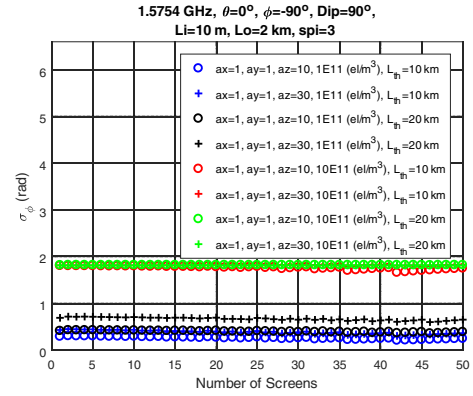

Figure 4. Results for phase scintillation versus the number of screens.

In order to quantify the number of screens required for the solutions to converge we analyzed the percent difference of the solutions obtained as more screens are used for a given irregularity thickness. The results for the amplitude and phase scintillation estimates are included in Figure 5 and Figure 6. It was found that for ΔN equal to $1^{11} el/m^3$ that a minimum of 10 screens is required for L_{th} equal to 10 km to achieve a 1 percent difference between solutions for S_4 estimates. When ΔN is equal to $10^{11} el/m^3$ a minimum of 15 screens is required for L_{th} equal to 20 km to achieve a 1 percent difference between solutions for S_4 estimates. When ΔN is equal to $1^{11} el/m^3$ a minimum of 3 screens is required for L_{th} equal to 10 km to achieve a 1 percent difference between solutions for σ_ϕ estimates. When ΔN is equal to $10^{11} el/m^3$ a minimum of 2 screens is required for L_{th} equal to 20 km to achieve a 1 percent difference between solutions for σ_ϕ estimates. It is also worth noting that in all instances that after solutions have converged that the addition of more screens leads to an apparent divergence of solutions. This divergence is particularly apparent for cases where az is equal to 10 and suggests a limitation to the FPE approximation utilized in the current version of SIGMA.

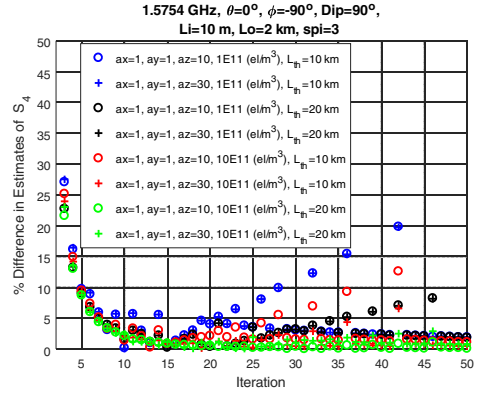

Figure 5. Percent difference between amplitude scintillation estimates as the number of layers is increased.

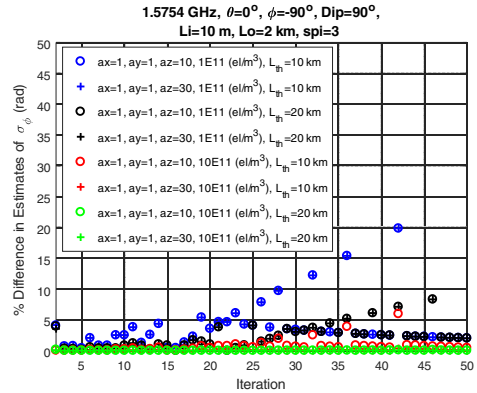

Figure 6. Percent difference between phase scintillation estimates as the number of layers is increased.

3 Conclusions

In this paper we have shown that for highly elongated vertical irregularities that phase scintillation solutions converge when using as few as 2 or 3 phase screens while as many as 10 to 15 screens are needed for amplitude scintillation estimates to converge. It was also shown that in all cases that after solutions have converged that the addition of more screens leads to an apparent divergence of solu-

tions which suggests a limitation to the FPE approximation utilized in the current version of SIGMA. While additional work is needed to better understand the relationship between SIGMA input parameters and the number of phase screens required for scintillation estimates to converge, the results of this work provide valuable insight and underscores the need to carefully analyze a phase screen model setup to achieve the accuracy required for a particular application given a set of input parameters.

4 Acknowledgements

The authors would like to acknowledge all the help and guidance they received on doing this work. AMDG.

References

References

[1] R. E. Collin, *Antennas and radiowave propagation*. McGraw-Hill series in electrical engineering, 1985.

[2] R. S. Lawrence, C. G. Little, and H. J. A. Chivers, "A survey of ionospheric effects upon earth-space radio propagation," *Proceedings of the IEEE*, vol. 52, no. 1, pp. 4–27, Jan 1964.

[3] "Ionospheric propagation data and prediction methods required for the design of satellite services and systems," *Recommendation ITU-R P.531-11*, 2012.

[4] D. L. Knepp and R. J. T., "Ionospheric environment and effects on space-based radar detection," in *Spaced-Based Radar Handbook*, L. J. Cantafio, Ed. Artech House Inc., 1989.

[5] K. C. Yeh and C.-H. Liu, "Radio wave scintillations in the ionosphere," *Proceedings of the IEEE*, vol. 70, no. 4, pp. 324–360, 1982.

[6] J. Aarons, "Global morphology of ionospheric scintillations," *Proceedings of the IEEE*, vol. 70, no. 4, pp. 360–378, 1982.

[7] Y. Jiao and Y. T. Morton, "Comparison of the effect of high-latitude and equatorial ionospheric scintillation on gps signals during the maximum of solar cycle 24," *Radio Science*, vol. 50, no. 9, pp. 886–903, Sept 2015.

[8] Y. Jiao, Y. T. Morton, S. Taylor, and W. Pelgrum, "Characterization of high-latitude ionospheric scintillation of gps signals," *Radio Science*, vol. 48, no. 6, pp. 698–708, 2013, 2013RS005259. [Online]. Available: http://dx.doi.org/10.1002/2013RS005259

[9] K. B. Deshpande, "Investigation of high latitude ionospheric irregularities utilizing modeling and gps observations," 2014.

[10] J. P. Conroy and K. Deshpande, "Satellite-beacon lonospheric-scintillation global model of the upper atmosphere (SIGMA): Enhancements and GPS signal propagation modeling," in *2017 XXXIInd General Assembly and Scientific Symposium of the International Union of Radio Science (URSI GASS)*, Aug 2017, pp. 1–4.

[11] C. Rino, *The Theory of Scintillation with Applications in Remote Sensing*. John Wiley & Sons, Inc., 2011.

[12] D. L. Knepp, "Multiple phase-screen calculation of the temporal behavior of stochastic waves," *Proceedings of the IEEE*, vol. 71, no. 6, pp. 722–737, June 1983.

[13] K. B. Deshpande, G. S. Bust, C. R. Clauer, C. L. Rino, and C. S. Carrano, "Satellite-beacon Ionospheric-scintillation Global Model of the upper Atmosphere (SIGMA) I: High-latitude sensitivity study of the model parameters," *Journal of Geophysical Research: Space Physics*, vol. 119, no. 5, pp. 4026–4043, 2014. [Online]. Available: http://dx.doi.org/10.1002/2013JA019699

[14] J. P. Conroy and K. Deshpande, "Satellite-beacon Ionospheric-scintillation Global Model of the upper Atmosphere (SIGMA): GNSS Signal Propagation Modeling and Channel Mismatch Analysis," in *2018 U.S. National Committee of the International Union of Radio Science (USNC-URSI)*, January 2018.

[15] C. S. Carrano, K. M. Groves, and R. G. Caton, "A phase screen simulator for predicting the impact of small-scale ionospheric structure on sar image formation and interferometry," in *Geoscience and Remote Sensing Symposium (IGARSS), 2010 IEEE International*, July 2010, pp. 162–165.

[16] P. A. Bernhardt, C. L. Siefring, I. J. Galysh, T. F. Rodilosso, D. E. Koch, T. L. MacDonald, M. R. Wilkens, and G. P. Landis, "Ionospheric applications of the scintillation and tomography receiver in space (citris) mission when used with the doris radio beacon network," *Journal of Geodesy*, vol. 80, no. 8, pp. 473–485, Nov 2006. [Online]. Available: https://doi.org/10.1007/s00190-006-0064-6

[17] K. B. Deshpande, G. S. Bust, C. R. Clauer, W. A. Scales, N. A. Frissell, J. M. Ruohoniemi, L. Spogli, C. Mitchell, and A. T. Weatherwax, "Satellite-beacon Ionospheric-scintillation Global Model of the upper Atmosphere (SIGMA) II: Inverse modeling with high-latitude observations to deduce irregularity physics," *Journal of Geophysical Research: Space Physics*, vol. 121, no. 9, pp. 9188–9203, 2016, 2016JA022943. [Online]. Available: http://dx.doi.org/10.1002/2016JA022943